HP-PbF_2-type FeCl_2 as a potential Cl-carrier in the deep Earth (Revision 1)

Hongsheng Yuan[1*], *Lianjie Man*[1], *Duck Young Kim*[1], *Dmitry Popov*[2], *Yue Meng*[2], *Eran Greenberg*[3¶], *Vitali Prakapenka*[3], *and Li Zhang*[1*]

[1]Center for High Pressure Science and Technology Advanced Research (HPSTAR), Shanghai 201203, China

[2]HPCAT, X-ray Science Division, Argonne National Laboratory, Argonne, IL 60439, U.S.A.

[3]GeoSoilEnviroCARS, University of Chicago, Chicago, Illinois 60637, USA.

*Corresponding author: Hongsheng Yuan(hongsheng.yuan@hpstar.ac.cn), Li Zhang (zhangli@hpstar.ac.cn)

¶ Present address: Earn Greenberg: Applied Physics Division, Soreq Nuclear Research Center (SNRC), Yavne 81800, Israel.

Abstract

We report for the first time the formation of a HP-PbF_2-type $FeCl_2$ phase (space group: $Pa\bar{3}$), through high pressure-temperature (*P-T*) reactions in the hydrous systems $(Mg_{0.6}Fe_{0.4})SiO_3$–H_2O–NaCl and FeO_2H–NaCl in a laser-heated diamond anvil cell up to 108 GPa and 2000 K. Applying single-crystal X-ray diffraction (XRD) analysis to individual submicron-sized grains, we have successfully determined the crystal structure of the as-synthesized $FeCl_2$ phase, in agreement with our theoretical structure search results. In-situ high *P-T* XRD data revealed the substitution of Cl for OH(O) in such a cubic $Pa\bar{3}$ symmetry, demonstrating that this topology is a potential host for both H and Cl in the deep Earth. The chemical analysis on the recovered sample showed a considerable Na_2O content and an abundance of ferric iron in the post-perovksite phase. The coexistence of the cubic $FeCl_2$ phase and post-perovksite suggests that the lowermost mantle could be a potential reservoir of Cl. The possible presence of volatiles such as H and Cl in the deep lower mantle would impact the composition and iron valence state of the post-perovksite phase.

Keywords: iron chloride, multigrain X-ray diffraction, lower mantle, hydrogen and chlorine cycle, post-pervoskite

Introduction

Cl is abundant in seawater and most geological fluids. Owing to its hydrophilic behavior, Cl aboundances and isotopic data provide important information on geological processes (Bonifacie et al. 2008; Sharp et al. 2010). Hydrous minerals have been shown to be major Cl carriers from oceanic to deep subduction environments (Kendrick et al. 2017). Serpentinites act as the major carriers of H (or H_2O) and Cl, and subducting serpentinites play an important role in the recycling of Cl (Scambelluri and Philippot 2001). Mass balance calculations suggest that Cl inputs exceed outputs at certain subduction zones (Barnes and Straub 2010; John et al. 2011). This is consistent with the observations of Mg-, Fe- and alkali-rich saline fluids containing up to 50 wt% Cl, Na, K, Mg and Fe trapped as inclusions inside high-pressure vein minerals in many eclogitic terranes, suggesting that Cl is recycling back into the mantle by subduction (Scambelluri et al. 1997).

There is a growing body of research that focuses on the storage potential of halogens and hydrogen in the mantle. Roberge et al. (2017) showed that the Cl contents in hydrous wadsleyite and ringwoodite ranging from 60 ±60 to 200 ±48 ppm are much lower than their F contents that range from 186 ±19 to 850 ±85 ppm, but that the substitution correlations of Cl^- with OH^- remain unclear. Yoshino & Jaseem (2018) found that incorporation of water and alumina greatly enhances F solubility in bridgmanite, exceeding 1 wt%, showing a sufficient capacity to store the whole F budget. The ionic radius of Cl^- is significantly larger than that of F^-, so that the Cl solubility in the mantle silicates is expected to be very low. The major host for Cl in the deep mantle remains unknown. Du et al. (2018) predict a series of stable structures of iron chlorides including Fe_3Cl, Fe_2Cl, FeCl, $FeCl_2$, $FeCl_3$ and $FeCl_4$ in the pressure range of Earth's mantle and core.

Recent studies showed that the pyrite-structured FeO_2 and FeO_2H_x ($x \leq 1$) phase was observed under *P-T* conditions representative of the deep lower mantle (DLM) (Hu et al. 2016; Liu et al. 2017; Mao et al. 2017; Nishi et al. 2017; Yuan et al. 2018). The latest study by E. Koemets et al. (2021) argued that FeO_2 and FeO_2H_x adopt HP-PdF_2-type other than pyrite-type structure due to the absense of the O–O covalent bonds. In spite of the controversy, we termed this cubic FeO_2H_x as “py-phase” in this work. As an important hydrogen carrier, the py-phase has been experimentally confirmed to be stable in the DLM along average mantle geotherm. Koemets et al. (2020) reported a novel $Na_2FeCl_4OH_x$ phase through chemical reactions between FeO_2H and NaCl under high *P-T* conditions. It is intriguing to explore the potential relation of hydrogen and chlorine in the Fe-bearing system in the DLM. Here we report the first experimental discovery of a cubic $FeCl_2$ phase, referred to as “c-$FeCl_2$”, coexisting with a post-perovskite (pPv) phase in the system (Mg,Fe)SiO_3–H_2O–NaCl. We demonstrated replacement of OH(O) by Cl in the cubic $Pa\bar{3}$ structure, providing a new hydrogen-chlorine relation under the *P-T* conditions of the DLM.

Methods

We used goethite (α-FeO_2H) powder (99+% purity, Alfa Aesar) and synthesized $Mg_{0.6}Fe_{0.4}SiO_3$ orthopyroxene (En60) as the starting samples.Three hydrous sample assemblies ($Mg_{0.6}Fe_{0.4}$)SiO_3(En60)–NaCl–H_2O (Run CHS06), En60–H_2O (Run CSb003) and α-FeO_2H–NaCl (Run ETR3) were designed for this study. In-situ synchrotron XRD experiments were performed at HPCAT (Sector 16) (Meng et al. 2015) and GeoSoilEnviroCARS (the University of Chicago, Sector 13) (Prakapenka et al. 2008), Advanced Photon Source (APS), Argonne National Laboratory. Decompression XRD experiments were performed at beamline 15U1, Shanghai Synchrotron Radiation Facility (SSRF), China. The starting assemblies, *P-T* conditions and heating duration are summarized in Table S1 in the supporting information. Complementary to the in-situ XRD characterization, ex-situ chemical analysis was performed on the recovered sample of Run CHS06 by a transmission electron microscope (TEM) coupled with an energy dispersive X-ray spectroscopy (EDS). We also conducted first-principles calculations to examine the stability, structure and electronic properties of $FeCl_2$ from the Fe–Cl system. See supporting information for details of methods.

Results and discussion

The sample assembly En60–NaCl–H_2O was compressed to 108(2) GPa at room *T* and heated at 1950(200) K, and we observed the appearance of the pPv phase along with several additional sharp peaks while the diffraction lines of NaCl vanished following heating (Fig. 1a and Fig. S1 in the supporting information), indicating a chemical reaction occurring in this system. For comparison, previous experiments on dry $(Mg,Fe)SiO_3$ orthopyroxene using NaCl medium under similar *P*-*T* conditions did not show any sign of reaction (e.g. Dorfman et al., 2013). To investigate the role of water in this reaction, we further conducted high *P*-*T* experiments on an assemblage of En60–H_2O without NaCl. As shown in Figure 1b, the diffraction peaks can be well indexed by the coexistence of the pPv and py-phase at 115(2) GPa after 2150(200) K heating, indicating a reaction between En60 and water. The py-phase has a lattice parameter of a= 4.3676(2) Å at 115 GPa and after *T* quench. Notably, the new peaks (marked by "C") observed in the system En60–NaCl–H_2O can be well indexed by a cubic lattice with a= 4.9490(2) Å at 108(2) GPa (Fig. 1a). The combined results suggest that the py-phase might react with NaCl under similar *P*-*T* conditions.

To examine the formation mechanism of the new cubic phase, we performed high *P*-*T* experiments on the assemblage of α-FeO_2H–NaCl. The sample was first compressed to around 100 GPa at room temperature. As shown in Fig. 2a, sharp peaks of the py-phase were observed within the first two minutes of heating at 1700(200) K. Increasing *T* to 2000(200) K and heating the sample for another two minutes, we observed the appearance of new peaks together with formation of crystalline ice X (Loubeyre et al. 1999) at the expense of the py-phase. The dominant new phase(s) were preserved after *T* quench together with small amounts of the residual py-phase (Fig. 2b). The residual py-phase was indexed with *a*= 4.4079(8) Å at 100(2) GPa, which is consistent with the values measured by previous studies (Nishi et al. 2017, Hu et al. 2016). Similar to the cubic phase found in the system En60–NaCl–H_2O at 108(2) GPa, a significant portion of the new peaks can be indexed by a cubic lattice with *a*= 4.9779(6) Å at 100(2) GPa (Fig. 2b). The remaining diffractions cannot be indexed straightforwardly. We carried out another high *P*-*T* XRD (Run CSa010) at 96(2) GPa, and the sample was heated at 2050(200) K for 10 minutes (Fig. 2c). No py-phase can be observed in this run and the diffraction (110) of NaCl-B2 phase is strong in intensity, suggesting that the long-time heating duration and/or a larger ratio of NaCl:FeO_2H at the interface leads to a complete reaction. As seen in Fig. 2c, except for ice X, NaCl and the new cubic phase with *a*= 4.9822(2) Å, there were strong unidentified diffractions at lower diffraction angle, and similar diffractions with less pronounced intensity were observed in Run ETR3 (Fig. 2b).

During the preparation of this paper, it has come to our attention that the interaction between FeO_2H and NaCl was explored by Koemets et al. (2020). Indeed, identification of the products is a complex isssue. They identified the products as a mixture of two orthorhombic phases. And one of the phases was determined with a chemical formula of $Na_2FeCl_4OH_x$ by single-crystal XRD analysis at 107(2) GPa after 2400(200) K heating. As shown in Fig. 2c, we found that the calculated diffraction positions of the $Na_2FeCl_4OH_x$ phase together with the new cubic phase could well match most of the diffractions of the products in our experiment Run CSa010. On the other hand, the other orthorhombic phase they proposed (denoted as "oI phase") was not present in the run products of our experiment. The applied lower *T* of 2000 K may result in the absence of the oI phase and the presence of a new cubic phase in the current study, whereas the opposite situation occurred by heating at a higher *T* of 2400 K in the study of Koemets et al (2020). The structure solutions for all the products in the system FeO_2H–NaCl should be further investigated but beyond the scope of this work.

Importantly, the new cubic phase with a= 4.95–4.98 Å is repeatably produced in the systems En60–NaCl–H_2O and FeO_2H–NaCl at pressures of 96–108 GPa. We applied the multigrain XRD technique to index individual grains of the new cubic phase, following the procedures described in a previous study (Zhang et al. 2019). The crystal structure of the cubic phase was determined without prior knowledge of its chemical composition. Only two atomic positions are required to be filled in the structure and we obtained a reasonable structure model by filling the positions with Fe and Cl, respectively, indicating the HP-PbF_2-type $FeCl_2$ (see supporting information for details of single-crystal refinements).

Our theoretical prediction at 100 GPa shows $FeCl_2$ and $FeCl_3$ are energetically stable, while $FeCl_4$ becomes close to the convex hull line (Fig. 3a). The calculated structure of the $FeCl_2$ phase is in agreement with the experimental results (Table S2 in the supporting information). With a DFT+U approach, the cubic $FeCl_2$ is calculated to be an indirect band gap semiconductor with 0.1 eV (Fig. 3b. See supporting information for electronic properties of HP-PdF_2-type $FeCl_2$). Stable phonon dispersion curves of $FeCl_2$ at 30 and 100 GPa in our calculations suggest the stability of HP-PdF_2-type $FeCl_2$ in a broad pressure range (Fig. 3c and d). Indeed, we found that the HP-PbF_2-type $FeCl_2$ phase is stable at ~29 GPa during decompression (Fig. S2 in the supporting information). Since unit-cell parameters of the coexisting py-phase and HP-PdF_2-type $FeCl_2$ in Run ETR3 are well consistent with the previous experimental and calculated values of the endmembers, respectively, solid solutions between these two phases appear unlikely to be formed.

Geophysical implications

Previous studies showed that both metallic Fe and Fe oxides react with H_2O, producing the py-phase in the DLM. Yuan et al. (2019) demonstrated the coexistence of the py-phase and a pPv phase in a simplified Fe^{3+}-bearing hydrous subducted slab composition. We further found that En60 with Fe^{2+} reacts with H_2O, producing the py-phase coexisting with a pPv phase. These combined results suggest that the py-phase can be generally formed by the redox reactions between water and Fe-bearing minerals with Fe in different valence states. With the addition of NaCl, the HP-PdF_2-type $FeCl_2$ was produced in place of the py-phase through high *P-T* reactions in the systems FeO_2H–NaCl and En60–H_2O–NaCl. In comparison, a chemical reaction between CO_2 and py-phase was observed in the Fe-C-O-H system, producing a tetrahedral carbonate phase $Fe_4C_3O_{12}$ at the expense of the py-phase above 2300 K (Boulard et al., 2018). Although the iron valence state of py-phase is still under debate, it is clear that the reaction product of $Fe_4C_3O_{12}$ contains only Fe^{3+} in the carbon-bearing system, while total Fe^{2+} is found for $FeCl_2$ in the chlorine-bearing system. These investigations suggest that the deep Earth volatile cycles including hydrogen, carbon and chlorine are correlated in a more complex way than previously thought, suggesting a volatile-dependent Fe^{2+}/Fe^{3+} ratio heterogeneity in the DLM.

The recent discovery of Ice-VII and halite inclusions in the deep mantle diamonds provides direct evidence for the existence of saline fluid in the shallow lower mantle at least regionally (Tschauner et al. 2018). A recent isotopic study showed that Cl-rich melt inclusions are associated with radiogenic Pb isotopes in the lower-mantle sourced olivine samples, indicating that surface Cl in the ancient seawater-altered and carbonated oceanic crust has been conveyed downward to the lower mantle (Hanyu et al. 2019). These geochemical and isotopic studies show that a considerable Cl (i.e 13–26% or an even greater proportion of the total Cl in the mantle) might have been cycled into lower mantle by slab subduction. However, Cl-bearing phases have not been identified so far in subducted oceanic crust beyond sub-arc depth. Our present results reveal that HP-PdF_2-type $FeCl_2$ phase is stable at depths beyond 30 GPa to the base of the lower mantle. Since Cl is incompatible with major minerals, Cl can possibily survive in mineral grain boundaries in a cold slab (Hiraga et al. 2004). When the Cl component interacts with hydrous Fe-bearing minerals at greater depths, forming HP-PdF_2-type $FeCl_2$ phase, this phase would potentially deliver Cl into the deep Earth.

The $Na_2FeCl_4OH_x$ phase can be observed in the system FeO_2H–NaCl but absent in the system En60–H_2O–NaCl. The Na component may go into the pPv phase. Indeed, our TEM-EDS results showed that the pPv phase in the En60–H_2O–NaCl system contains ~3 wt.% Na_2O (Fig.S3 and Table S3 in the supporting information). Considering the pPv phase with a chemical formula on the join $[(Mg,Fe^{2+})_{1-x}(Fe^{3+},Fe^{3+})_{2x}Si_{1-x}O_3]$–$Na_2SiO_3$, the abundance of ferric iron (Fe^{3+}/total Fe ratio) is estimated to be ~0.6. Hirose et al. (2005) showed that 5 wt.% Na_2O together with a high Fe^{3+}/total Fe ratio up to 0.8 is incorporated in the pPv phase with a Mid Ocean Ridge Basalt starting composition. Therefore, the presence of volatiles such as H and Cl would impact the composition and iron valence state of the pPv phase in the DLM. Furthermore, we found a possible partial melt coexisting with pPv and $FeCl_2$ from the combined high *P*-*T* XRD and chemical analysis results. Such a volatile-assisted melting process in the DLM may account for the seismic observations such as ultralow velocity zones (Ren et al. 2007) and large low-shear-velocity provinces (Ford et al. 2006).

Acknowledgments

The authors acknowledge the support from the National Natural Science Foundation of China (NSFC) (Grant No: 41902033, 41574080, 11774015 and U1530402). This work was performed at HPCAT (Sector 16) and GeoSoilEnviroCARS (The University of Chicago, Sector 13), Advanced Photon Source (APS), Argonne National Laboratory. HPCAT operations are supported by DOE-NNSA's Office of Experimental Sciences. GeoSoilEnviroCARS is supported by the National Science Foundation-Earth Sciences (EAR-1634415) and Department of Energy-GeoSciences (DE-FG02-94ER14466). The Advanced Photon Source is a U.S. Department of Energy (DOE) Office of Science User Facility operated for the DOE Office of Science by Argonne National Laboratory under Contract No. DE-AC02-06CH11357. Portions of this work were performed at the beamline 15U1 of the Shanghai Synchrotron Radiation Facility (SSRF).

References

Barnes, J.D., and Straub, S.M. (2010) Chorine stable isotope variations in Izu Bonin tephra: Implications for serpentinite subduction. Chemical Geology, 272, 62–74.

Bonifacie, M., Jendrzejewski, N., Agrinier, P., Humler, E., Coleman, M., and Javoy, M. (2008) The chlorine isotope composition of earth's mantle. Science, 319, 1518–1520.

Boulard, E., Guyot, F., Menguy, N., Corgne, A., Auzende, A.L., Perrillat, J.P., and Fiquet, G. CO_2-induced destabilization of pyrite-structured FeO_2H_x in the lower mantle. National Science Review, 5, 870–877.

Dorfman, S.M., Meng, Y., Prakapenka, V.B., and Duffy, T.S. (2013) Effects of Fe-enrichment on the equation of state and stability of (Mg,Fe)SiO_3 perovskite. Earth and Planetary Science Letters, 361, 249–257.

Du, X., Wang, Z., Wang, Hongbo, Iitaka, T., Pan, Y., Wang, Hui, and Tse, J.S. (2018) Structures and Stability of Iron Halides at the Earth's Mantle and Core Pressures: Implications for the Missing Halogen Paradox. ACS Earth and Space Chemistry, 2, 711–719.

Ford, S.R., Garnero, E.J., and McNamara, A.K. (2006) A strong lateral shear velocity gradient and anisotropy heterogeneity in the lowermost mantle beneath the southern Pacific. Journal of Geophysical Research: Solid Earth, 111, 1–14.

Hanyu, T., Shimizu, K., Ushikubo, T., Kimura, J.I., Chang, Q., Hamada, M., Ito, M., Iwamori, H., and Ishikawa, T. (2019) Tiny droplets of ocean island basalts unveil Earth's deep chlorine cycle. Nature Communications, 10, 4–10.

Hiraga, T., Andeson, I.M., and Kohlstedt, D.L. (2004) Grain boundaries as reservoirs of incompatible elements in the Earth's mantle. Nature, 427, 699–703.

Hirose, K., Takafuji, N., Sata, N., and Ohishi, Y. (2005) Phase transition and density of subducted MORB crust in the lower mantle. Earth and Planetary Science Letters, 237, 239–251.

Hu, Q., Kim, D.Y., Yang, W., Yang, L., Meng, Y., Zhang, L., and Mao, H.-K. (2016) FeO_2 and FeOOH under deep lower-mantle conditions and Earth's oxygen–hydrogen cycles. Nature, 534, 241–244.

John, T., Scambelluri, M., Frische, M., Barnes, J.D., and Bach, W. (2011) Dehydration of subducting serpentinite: Implications for halogen mobility in subduction zones and the deep halogen cycle. Earth and Planetary Science Letters, 308, 65–76.

Kendrick, M.A., Hémond, C., Kamenetsky, V.S., Danyushevsky, L., Devey, C.W., Rodemann, T., Jackson, M.G., and Perfit, M.R. (2017) Seawater cycled throughout Earth's mantle in partially serpentinized lithosphere. Nature Geoscience, 10, 222–228.

Koemets, E., Yuan, L., Bykova, E., Glazyrin, K., Ohtani, E., and Dubrovinsky, L. (2020) Interaction Between FeOOH and NaCl at Extreme Conditions: Synthesis of Novel Na2FeCl4OHx Compound. Minerals, 10, 51.

Koemets, E., Leonov, I., Bykov, M., Bykova, E., Chariton, S., Aprilis, G., Fedotenko, T., Clément, S., Rouquette, J., Haines, J., and others (2021) Revealing the Complex Nature of Bonding in the Binary High-Pressure Compound FeO_2. Physical Review Letters, 126, 1–7.

Liu, J., Hu, Q., Young Kim, D., Wu, Z., Wang, W., Xiao, Y., Chow, P., Meng, Y., Prakapenka, V.B., Mao, H.K., and others (2017) Hydrogen-bearing iron peroxide and the origin of ultralow-velocity zones. Nature, 551, 494–497.

Loubeyre, P., LeToullec, R., Wolanin, E., Hanfland, M., and Hausermann, D. (1999) Modulated phases and proton centring in ice observed by X-ray diffraction up to 170 GPa. Nature, 397, 503–506.

Mao, H., Hu, Q., Yang, L., Liu, J., Kim, D.Y., Meng, Y., Zhang, L., Prakapenka, V.B., Yang, W., and Mao, W.L. (2017) When water meets iron at Earth's core-mantle boundary. National Science Review, 4, 870–878.

Meng, Y., Hrubiak, R., Rod, E., Boehler, R., and Shen, G. (2015) New developments in laser-heated diamond anvil cell with in situ synchrotron x-ray diffraction at High Pressure Collaborative Access Team. Review of Scientific Instruments, 86, 072201.

Nishi, M., Kuwayama, Y., Tsuchiya, J., and Tsuchiya, T. (2017) The pyrite-Type high-pressure form of FeOOH. Nature, 547, 205–208.

Prakapenka, V.B., Kubo, A., Kuznetsov, A., Laskin, A., Shkurikhin, O., Dera, P., Rivers, M.L., and Sutton, S.R. (2008) Advanced flat top laser heating system for high pressure research at GSECARS: Application to the melting behavior of germanium. High Pressure Research, 28, 225–235.

Ren, Y., Stutzmann, E., van der Hilst, R.D., and Besse, J. (2007) Understanding seismic heterogeneities in the lower mantle beneath the Americas from seismic tomography and plate tectonic history. Journal of Geophysical Research: Solid Earth, 112, 1–15.

Roberge, M., Bureau, H., Bolfan-Casanova, N., Raepsaet, C., Surble, S., Khodja, H., Auzende, A.L., Cordier, P., and Fiquet, G. (2017) Chlorine in wadsleyite and ringwoodite: An experimental study. Earth and Planetary Science Letters, 467, 99–107.

Scambelluri, M., and Philippot, P. (2001) Deep fluids in subduction zones. Lithos, 55, 213–227.

Scambelluri, M., Piccardo, G., Philippot, P., Robbiano, A., and Negretti, L. (1997) High salinity fluid inclusions formed from recycled seawater in deeply subducted alpine serpentinite. Earth and Planetary Science Letters, 148, 485–499.

Sharp, Z.D., Shearer, C.K., McKeegan, K.D., Barnes, J.D., and Wang, Y.Q. (2010) The Chlorine Isotope Composition of the Moon and Implications for an Anhydrous Mantle. Science, 329, 1050–1053.

Tschauner, O., Huang, S., Greenberg, E., Prakapenka, V.B., Ma, C., Rossman, G.R., Shen, A.H., Zhang, D., Newville, M., Lanzirotti, A., and others (2018) Ice-VII inclusions in diamonds: Evidence for aqueous fluid in Earth's deep mantle. Science, 359, 1136–1139.

Yoshino, T., and Jaseem, V. (2018) Fluorine solubility in bridgmanite : A potential fluorine reservoir in the Earth ' s mantle. Earth and Planetary Science Letters, 504, 106–114.

Yuan, H., Zhang, L., Ohtani, E., Meng, Y., Greenberg, E., and Prakapenka, V.B. (2019) Stability of Fe-bearing hydrous phases and element partitioning in the system $MgO–Al_2O_3–Fe_2O_3–SiO_2–H_2O$ in Earth's lowermost mantle. Earth and Planetary Science Letters, 524, 115714.

Yuan, L., Ohtani, E., Ikuta, D., Kamada, S., Tsuchiya, J., Naohisa, H., Ohishi, Y., and Suzuki, A. (2018) Chemical Reactions Between Fe and H_2O up to Megabar Pressures and Implications for Water Storage in the Earth's Mantle and Core. Geophysical Research Letters, 45, 1330–1338.

Zhang, L., Yuan, H., Meng, Y., and Mao, H. (2019) Development of High-Pressure Multigrain X-Ray Diffraction for Exploring the Earth's Interior. Engineering, 5, 441–447.

Figure Captions

Figure 1. Experimental evidence for (a) CHS06: $Mg_{0.6}Fe_{0.4}SiO_3$–H_2O–NaCl and (b) CSb003: $Mg_{0.6}Fe_{0.4}SiO_3$–H_2O. (a) Coexistence of pPv and a previously unknown cubic phase (marked by "C") at 108(2) GPa after *T* quench from 1950 K: PPv, *a*=2.482(3) Å, *b*=8.217(14) Å, *c*=6.177(2) Å; C*, a*=4.9490(2) Å. (b) Coexistence of pPv and py-FeO_2H phase at 115(2) GPa after *T* quench from 2150 K: pPv, *a*=2.484(2) Å, *b*=8.155(12) Å, *c*=6.171(5) Å;.py, *a*=4.3676(2) Å. The calculated peak positions are indicated by ticks. Portions of corresponding spotty XRD patterns of the runs are shown in (c) CHS06 and (d) CSb003, respectively. Experiments were performed with a X-ray wavelength of 0.3344 Å at 13-IDD, APS.

Figure 2. Experimental evidence for chemical reaction between α-FeO_2H and NaCl under high *P-T* conditions. (a) XRD patterns obtained around 100 GPa at 1700 K (formation of py-phase) and at 2000 K (formation of the "C" phase together with ice X). XRD patterns for (b) Run ETR3 at 100(2) GPa and (c) Run CSa010 at 96(2) GPa after *T* quench. The peak positions of the two orthorhombic phases, the $Na_2FeCl_4OH_x$ phase (space group: *Pbam*) (marked by "N") with *a* = 8.725(2) Å, *b* = 6.180(3) Å, *c* = 3.0679(12) Å and the oI phase (space group: *Imm*2) with *a* = 2.5467(5) Å, *b* = 9.640(2) Å, *c* = 11.580(2) Å at 107(2) GPa from the study by Koemets et al. (2020) are indicated with magenta and orange ticks, respectively, in panel c. Experiments were performed with X-ray wavelengths of 0.4066 and 0.3445 Å for Runs ETR3 and CSa010, respectively, at 16-IDB, APS. The X-axis was set as Q values ($Q = \frac{4\pi\sin\theta}{\lambda}$), where θ and λ represent the diffraction angle and X-ray wavelength, respectively.

Figure 3. Computational results of the high-pressure PbF_2-type $FeCl_2$ phase. (a) Convex hull results of various Fe-Cl at 100 GPa. (b) electronic structure dispersion relations of $FeCl_2$ at 100

GPa with a Fermi level set to 0 (blue dashed line). Harmonic phonon dispersion of $FeCl_2$ at (c) 30 GPa and (d) 100 GPa.

1

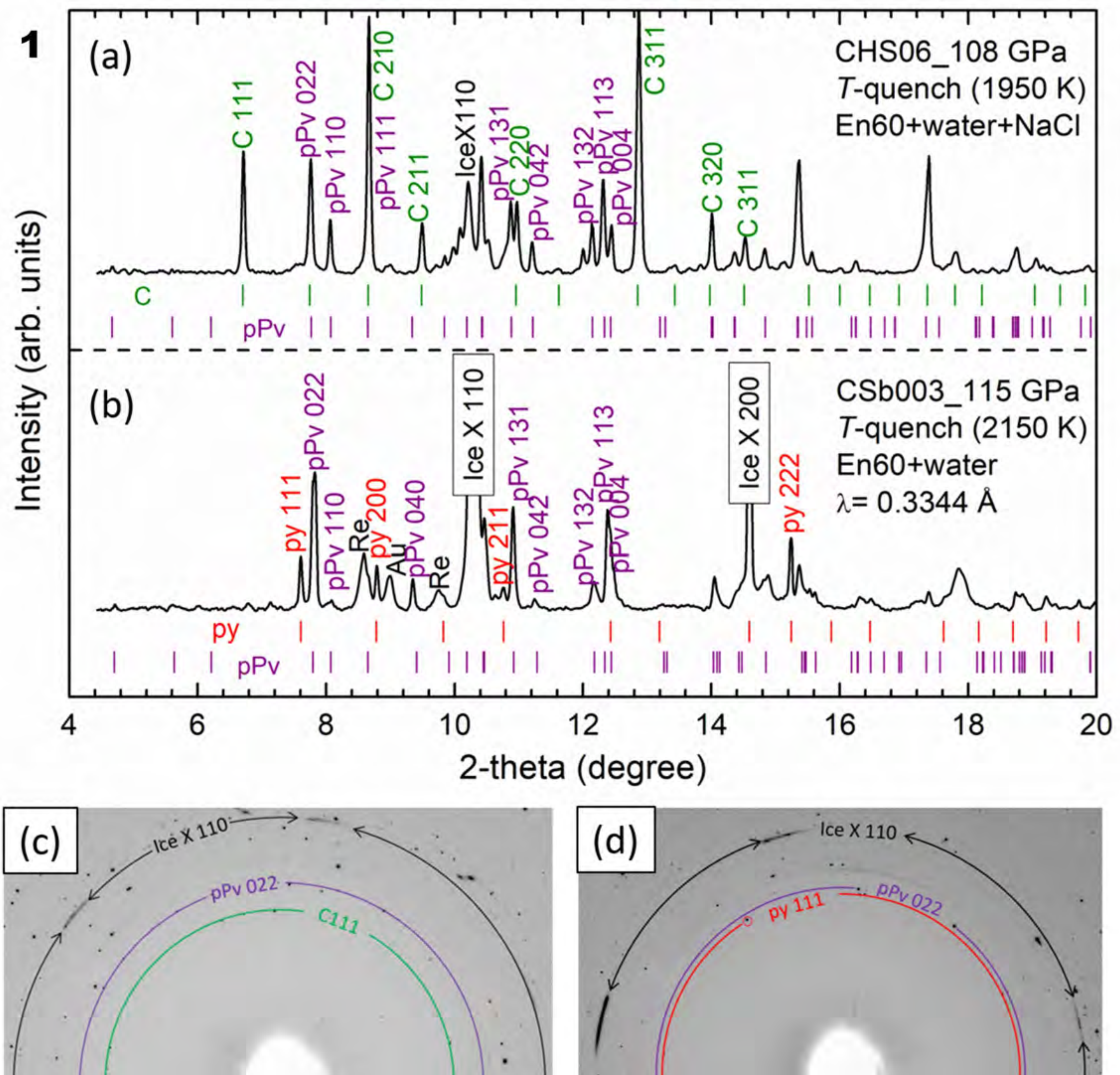
(a)
CHS06_108 GPa
T-quench (1950 K)
En60+water+NaCl
C 111
pPv 022
pPv 110
pPv 111
C 210
C 211
IceX110
pPv 131
C 220
pPv 042
pPv 132
pPv 113
pPv 004
C 311
C 320
C 311
C
pPv
(b)
CSb003_115 GPa
T-quench (2150 K)
En60+water
λ= 0.3344 Å
py 111
pPv 022
pPv 110
Re
py 200
Au
pPv 040
Re
Ice X 110
py 211
pPv 131
pPv 042
pPv 132
pPv 113
pPv 004
Ice X 200
py 222
py
pPv
Intensity (arb. units)
2-theta (degree)
4
6
8
10
12
14
16
18
20
(c)
Ice X 110
pPv 022
C111
(d)
Ice X 110
pPv 022
py 111

2

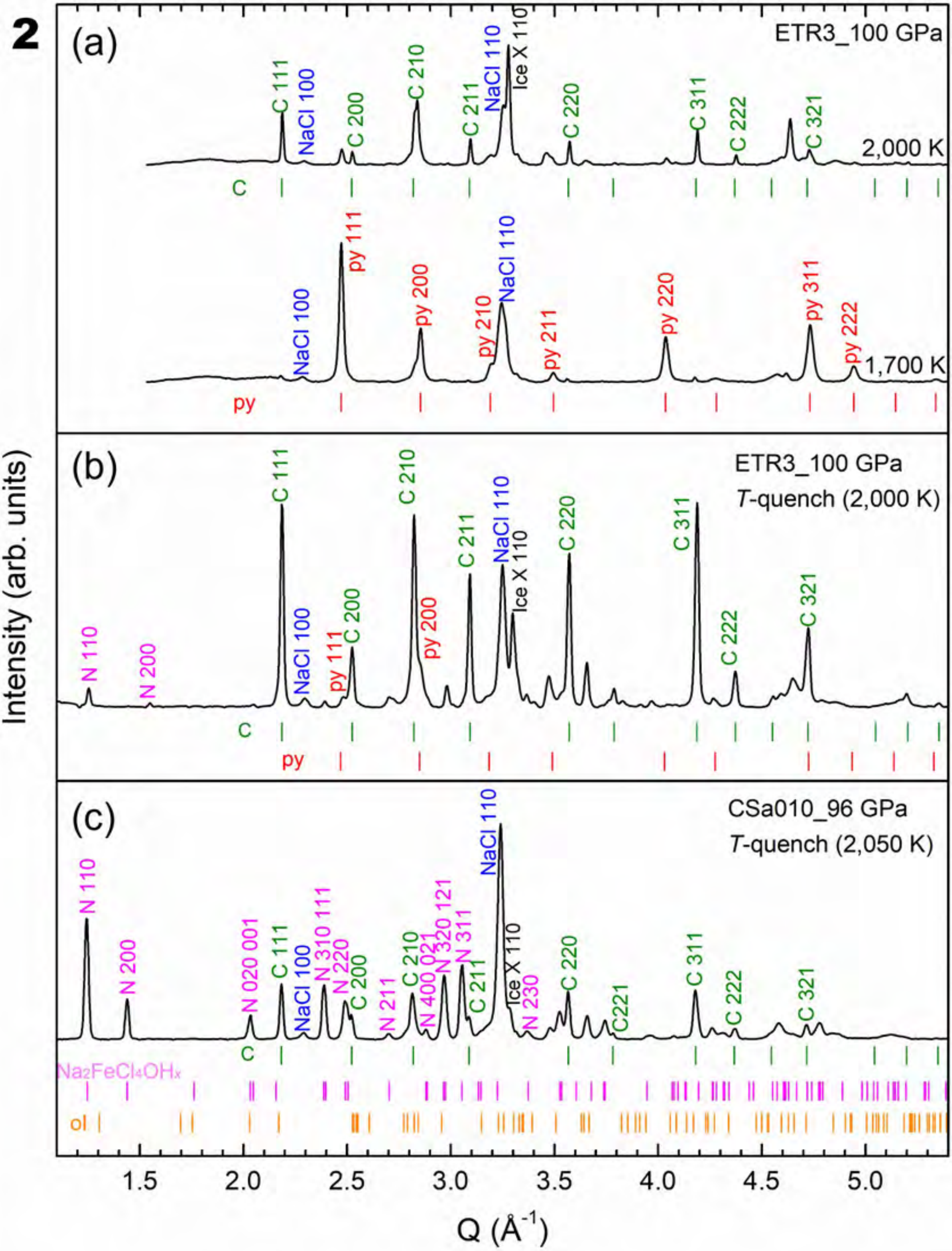

(a)
ETR3_100 GPa
2,000 K
C 111
NaCl 100
C 200
C 210
C 211
NaCl 110
Ice X 110
C 220
C 311
C 222
C 321
C
1,700 K
NaCl 100
py 111
py 200
py 210
NaCl 110
py 211
py 220
py 311
py 222
py
(b)
ETR3_100 GPa
T-quench (2,000 K)
N 110
N 200
C 111
NaCl 100
py 111
C 200
C 210
py 200
C 211
NaCl 110
Ice X 110
C 220
C 311
C 222
C 321
C
py
(c)
CSa010_96 GPa
T-quench (2,050 K)
N 110
N 200
N 020 001
C 111
NaCl 100
N 310 111
N 220
C 200
N 211
C 210
N 400 021
N 320 121
N 311
C 211
NaCl 110
Ice X 110
N 230
C 220
C221
C 311
C 222
C 321
C
Na2FeCl4OHx
ol
Intensity (arb. units)
1.5
2.0
2.5
3.0
3.5
4.0
4.5
5.0
Q (Å-1)

3

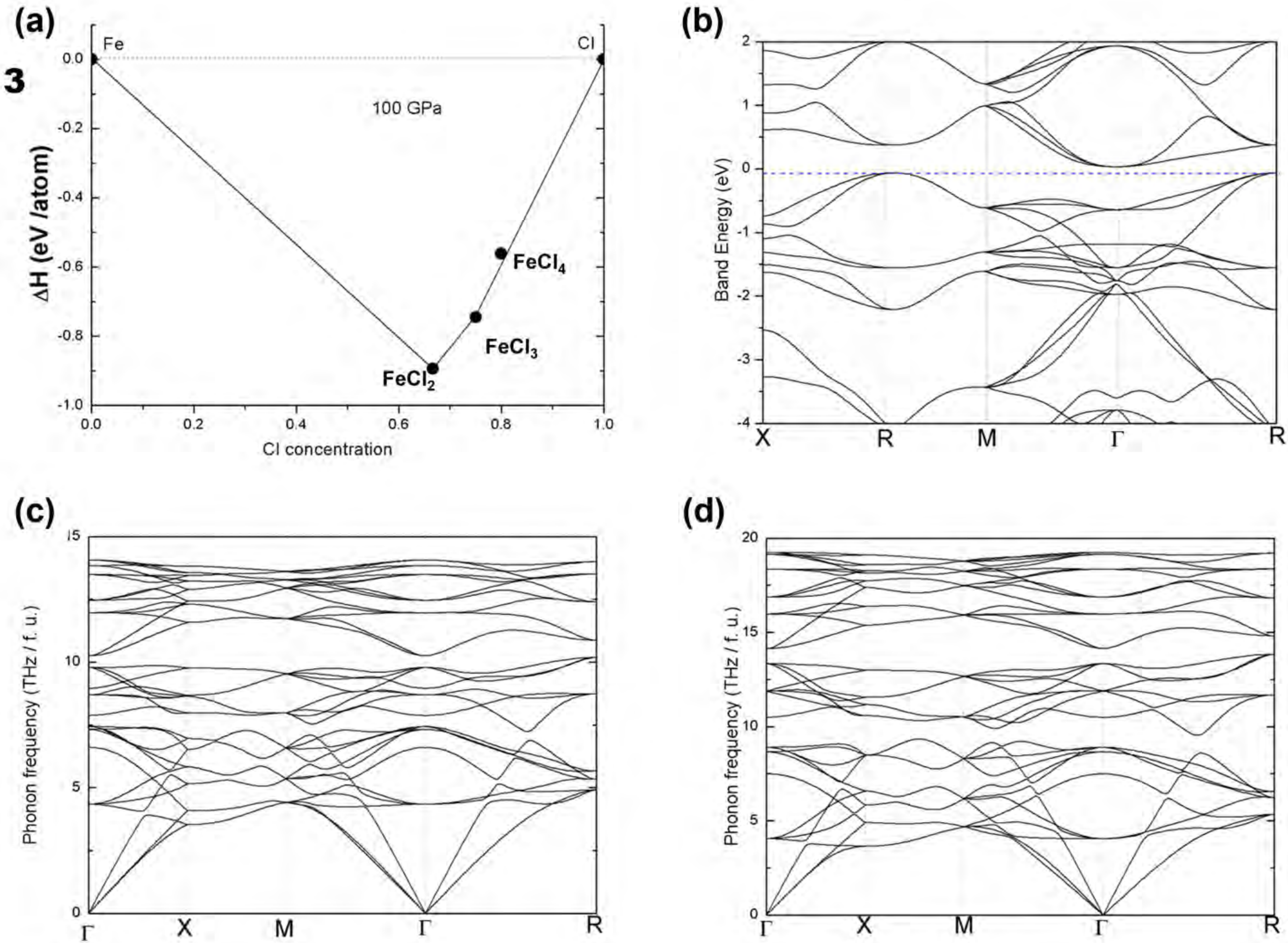
(a)
Fe
Cl
100 GPa
ΔH (eV /atom)
FeCl$_4$
FeCl$_3$
FeCl$_2$
Cl concentration
0.0
-0.2
-0.4
-0.6
-0.8
-1.0
0.0
0.2
0.4
0.6
0.8
1.0
(b)
Band Energy (eV)
2
1
0
-1
-2
-3
-4
X
R
M
Γ
R
(c)
Phonon frequency (THz / f. u.)
15
10
5
0
Γ
X
M
Γ
R
(d)
Phonon frequency (THz / f. u.)
20
15
10
5
0
Γ
X
M
Γ
R